Analysis of Scanning Tunneling Spectroscopy Experiments from First Principles: the Test Case of C_{60} Adsorbed on Au(111) **

Ángel J. Pérez-Jiménez,* Juan J. Palacios, Enrique Louis, Emilio SanFabián, José A. Vergés

February 6, 2008

[*] Dr. A. J. Pérez-Jiménez, Prof. E. SanFabián
Departamento de Química Física, Universidad de Alicante
San Vicente del Raspeig, Alicante E-03080 (Spain)
Fax: (+34)965903537
E-mail: AJ.Perez@ua.es

Prof. J. J. Palacios, E. Louis
Departamento de Física Aplicada, Universidad de Alicante (Spain)

Prof. J. A. Vergés
Instituto de Ciencia de Materiales de Madrid, *CSIC* (Spain)

[**] The authors wish to thank Drs. C. Rogero and J. I. Pascual for critically reading the manuscript and providing us with the experimental results shown in this paper. Financial support from Spanish DGICYT and the Generalitat Valenciana under Grants Nos. PB96-0085, GV00-151-01 and GV00-095-2 is gratefully acknowledged.

Many of the technological applications of fullerenes and their derivatives, either as lubricants, non-linear optical devices, superconductors or in molecular nanodevices depend on the use of thin films or the interaction with metal surfaces. This explains the tremendous effort that has been devoted by a number of researchers to understand and characterize C_{60} adlayers over a wide range of surfaces, usually by means of Scanning Tunneling Microscopy/Spectroscopy (STM/S) as well as with other spectroscopic techniques (See the work by Rogero *et al*[1] and references therein). Nevertheless STM/S data are sometimes difficult to interpret without aid from theoretical models. STM images and STS spectra are usually rationalized simplifying Bardeen's first-order formalism[2] by approximating the electronic structure of the tip[3] and that of the sample, as well as the tip-sample interaction.[4, 5, 6] On the other hand, single electron tunneling effects such as the Coulomb blockade and Coulomb staircase are accounted for by fits to simplified expressions derived from the golden-rule.[7, 8, 9] Each of the aforementioned methods has its *pros* and *cons*, but none of them combines the following two highly desirable characteristics: First, to overcome Bardeen's approximation in favor of Landauer's formalism.[10] This would allow a widening of the analysis range beyond the tunneling regime down to tip-substrate contact. Second, to be fully *ab initio*, without resorting to *ad hoc* parameters and approximations to describe the interaction between the adsorbed molecule, the substrate, and the tip. It is only in this way that a method can gain reliability and predictibility when *reproducing* STM/STS experiments.

We propose here a method that brings these two major premises together and which has successfully been applied previously to the characterization of the conductance properties in molecular nanodevices of the type metallic electrode + molecule + metallic electrode.[11, 12, 13] The procedure, which is termed *Gaussian Embedded Cluster Method* (GECM), computes Landauer's conductance formula through a divide-and-conquer scheme. This means that the electronic structure of the molecule and part of the electrodes is considered in full depth from first principles, since it embraces the most important region, while the semi-infinite non-periodic structure of the metal is treated with an efficient recursive model. Herein we report its capabilities studying adsorbed Buckminster fullerene on a gold surface, where recent and accurate STM/S experiments are available.[1]

Nucleation and growth of C_{60} monolayers and thin films on Au(111) surfaces has been widely studied.[14, 15, 16, 17, 18, 19] Although binding between gold and C_{60} is weaker than with other metals,[17, 20, 19] it is far from negligible; the adsorption energy is estimated around 40-60 kcal/mol.[15, 19] In fact, adsorption of C_{60} is able to lift the well-known $23 \times \sqrt{3}$ Au(111) reconstruction, and photoemission studies of C_{60} on polycrystalline Au[21, 22] and Au(111) surfaces[19] revealed energy shifts indicative of LUMO hybridization and charge transfer from Au to the adsorbed fullerene molecule. At high coverages, closed-packed layers grow with the thermodynamically most stable adsorbate phase being a $(2\sqrt{3} \times 2\sqrt{3})\ R30^o$ structure with a nearly perfect lattice matching in which all the molecules are in equivalent surface sites.[15]

Apart from this, another superstructure forms with crystallographic directions matching those of the substrate, resulting in fullerene molecules sitting on different adsorption sites.[15, 17] The proposed 11×11 C_{60} coverage[15, 17] for this superstructure has been recently discovered to be composed of a smaller 2×2 grid by Rogero *et al.*[1] In the following, we will focus on the characteristics of this superstructure as interpreted by Rogero *et al.*[1] which serve as an excellent benchmark for our calculations to be compared with.

The main features that characterize the adsorption of the above-mentioned C_{60} adlayers can be drawn from Figure 1, where we show the STS data obtained by Rogero *et al.*[1] from Current Imaging Tunneling Spectroscopy (CITS) measurements. This technique measures the tunneling current at each point during a topographic scan for a range of bias voltages applied to the sample-tip system. The numerical differentiation of each curve provides the corresponding conductance profile. From these curves it is possible to construct an image of the conductance at a given bias for each point like the one appearing in the right panel of Figure 1, which was obtained at a bias of +0.6V.[1] The curves plotted in the left panel of Figure 1 correspond to the conductance profiles measured at the points indicated with the circle and triangle.[1] As deduced from Figure 1 the differences in brightness between adsorbed C_{60} molecules in the CITS image correspond to differences in conductance height of the peaks appearing in the conductance profile. On the other hand, the relatively weak C_{60}-Au(111) binding reflects on the sharp form of the peaks, with the energetic position of the C_{60} LUMO level

shifted towards the Fermi level by charge transfer from the substrate, with a HOMO-LUMO gap of 2.3 eV. The two curves appearing in the left panel of Figure 1 are interpreted[1] as corresponding to a 2×2 superstructure of the adsorbed layer that places the C_{60} molecules on two different adsorption sites of the underlying substrate surface (see Figures 1, 3 and 4). According to this picture, C_{60} molecules sit alternatively onto bridge and on-top sites, the different interaction of the fullerene with the adsorption site being responsible for the two type of spectra. Henceforth, when a C_{60} molecule sits on top of a gold atom, where the interaction is supposed to be weaker, we end up with the *bright* peak, which is sharper than that corresponding to the molecule sitting on a bridge between two gold atoms, where the stronger interaction with the substrate would explain the increased width of the peak. The above site-specific properties are consistent with a larger displacement to the Fermi level of the peak corresponding to the bridge site with respect to that of the on-top one since the amount of charge transferred to the molecule is larger in the former than in the latter.

The characteristics and interpretation outlined in the preceding paragraph have been confirmed by our calculations as can be seen after inspecting Figure 2 where we plot the conductance profile corresponding to the two geometries that characterize the 2×2 C_{60} superstructure. Since the interaction between the molecule and the surface is not very strong, the conductance peaks reveal the underlying positioning of the C_{60} orbitals, from which we estimate the HOMO-LUMO gap to be 2.9 eV, in good accordance with the

experimental STS results.[1] The relative positioning and height of the conductance maxima between the on-top and bridge geometries is also reproduced. The form of the peaks reflects, as suggested by Rogero *et al.*,[1] the different interaction of the molecules with the adsorption sites as deduced from the Potential Energy Scan (PES) shown in Figure 5. For each adsorption site we plot Density Functional Theory (DFT) calculations when a C_{60} molecule approaches the Au(111) surface towards the on-top and bridge sites, respectively, with either a six-member ring or a five-member ring facing the surface. The same equilibrium distance (2.75Å) is obtained for all the geometries which coincides with that found in C_{60}-gold nanobridges[23] and is consistent with Altman and Colton suggestion of no height differences between adsorbed C_{60} molecules on Au(111).[15, 16] As seen from Figure 5 the adsorption energy is smaller when the molecule sits on top of a gold atom (16 kcal/mol) than when the fullerene binds to a bridge site (35 kcal/mol), which explains the narrower and higher form of the conductance maximum corresponding to the on-top geometry with respect to the bridge site. Once the aforementioned values are corrected by considering the lateral interaction of the C_{60} monolayer [19], estimated from the Lennard-Jones potential to be of about 25 kcal/mol[19], they lie within the experimental margins discussed above. The stronger Au-C_{60} interaction when the molecule sits on the bridge site is consistent with a larger amount of charge transferred from the gold surface to the molecule: 0.8 electron, as compared to the value of 0.5 electron obtained for the on-top site. This gap accounts for the different alignment

of the Fermi level, which for the bridge geometry lies closer to the LUMO-derived orbitals, in complete agreement with Rogero *et al.* findings. The amount of transferred charge calculated by us is in accordance with recent results derived from photoemission spectra[19], which give 0.8±0.2 electrons per fullerene molecule adsorbed on Au(111). Finally, we point out the fact that there exist minor differences in binding energy with respect to the symmetry axis that points towards the surface. Actually, this coincides with the fact that no predominant molecular orientation had been found[1] and is also indicative of the relative weak C_{60}-Au(111) interaction, which allows a large degree of rotational freedom on the adsorbed fullerene.

As mentioned before, our method is not only applicable to the tunneling regime but also at tip-sample contact distances. This is reflected in Figure 6 where we plot the conductance of the system for the two types of adsorption sites as the tip moves towards the adsorbed C_{60}. The two maxima correspond to conductance channels coming from the first three C_{60} LUMO-derived orbitals, whose degeneracy has been partially removed due to the interaction with the gold surface[1, 19] in two sets of two (broader peak) and one (sharper peak) resonances, respectively. These two peaks also appear at tunnel tip-surface distances in the experimental STS data of Rogero *et al.* (see Figure 1). We can check that, as the tip comes in closer contact with the fullerene, their interaction alters the size, width and positioning of the peaks. The net result is an increase in the conductance to non-negligible values and a larger shift of the LUMO-derived C_{60} orbitals towards the Fermi level due to

the larger amount of charge transferred from the tip atoms to the fullerene as they approach each other. This fact explains the slight closure of the HOMO-LUMO gap as the tip approaches the molecule, which is apparent after inspecting the insets of Figure 6. On the other hand, the relative shape of the peaks corresponding to the on-top and bridge geometries found at tunneling distances is maintained as the tip approaches the sample. This still reflects the differences in binding strength commented above. Figure 7 shows the value of the conductance maxima of the second peak *vs.* tip-surface distance. We can see the change of slope due to the different conductance regimes, with the exponential decay typical of tunneling appearing beyond 13Å, which agrees well with the experimental value reported by Joachim *et al.*[6] of 13.2Å. The departure from a linear trend in the logarithmic representation of the conductance is related to the above-mentioned closure of the C_{60} HOMO-LUMO gap. Structural deformation of the fullerene cage has not been considered in our calculations since we have focused on the change from tunneling to contact regimes, where the deformation of C_{60} by the tip is negligible.[6]

In summary, we have shown that the so-called GECM method is able to accurately reproduce STS spectra. The example of C_{60} adsorbed on Au(111) represents just a good and difficult starting point, but the method looks promising as a valuable tool in the interpretation of STM and STS spectra up to the contact regime.

Methods

Here we give a brief overview of our method; the interested reader is referenced to our earlier work.[11, 12, 13] Our procedure aims at a first-principles implementation of Landauer's conductance formula:

$$\mathcal{G} = \frac{2e^2}{h}\mathrm{Tr}[\hat{\Gamma}_L \hat{G}^r \hat{\Gamma}_R \hat{G}^a]. \tag{1}$$

In this equation, the operators $\hat{\Gamma}_L$ and $\hat{\Gamma}_R$ are built from the corresponding retarded, $\hat{\Sigma}^r$, and advanced $\hat{\Sigma}^a$, self-energy operators of the left (L) and right (R) electrodes according to:

$$\hat{\Gamma}_{L(R)} = i(\hat{\Sigma}^r_{L(R)} - \hat{\Sigma}^a_{L(R)}), \tag{2}$$

while $\hat{G}^r$ and $\hat{G}^a$ denote the retarded and advanced Green's functions operators, respectively, of the whole system and where Tr represents the trace over the pertinent orbitals. Simple as it looks, Landauer's formalism poses a challenging problem since the calculation of $\hat{\Sigma}$ involves the electronic structure of a semi-infinite non-periodic metallic electrode while $\hat{G}$ must deal with the intricacies of the metal-molecule interaction which, in turn, largely depends on the type and positions of the atoms involved.

Our approach to the problem consists of a divide-and-conquer scheme. First, we perform a DFT calculation of the molecule *including part of the leads with the desired geometry*: see Figures 3 and 4, where the two clusters representing the relevant part of the bridge and on-top geometries discussed above are depicted. We mention in passing that the DFT calculations were

performed by using the GAUSSIAN98[24] code with the B3LYP exchange-correlation functional[25] and the basis sets and Pseudopotentials of Christiansen *et al.*[26, 27] This is also the case for the DFT calculations that led to the PES of Figure 5 where clusters similar to those in Figures 3 and 4 were used, but with the five tip atoms removed. Additional clusters with the five-fold axis perpendicular to the surface were also used to derive the corresponding PES of Figure 5 but are not shown for convenience.

Since the Hamiltonian of the cluster representing the nanobridge, $\hat{H}$, is finite, its associated Green's functions are unsuitable for any current determination. In order to transform this finite system into an effectively infinite one we must include the self-energy of the electrodes:

$$[(\epsilon + i\delta)\hat{I} - \hat{H} - \hat{\Sigma}^r(\epsilon)]\hat{G}^r(\epsilon) = \hat{I} \tag{3}$$

where

$$\hat{\Sigma}^r = \hat{\Sigma}^r_R + \hat{\Sigma}^r_L. \tag{4}$$

The added self-energy is determined through a Bethe lattice tight-binding model[28, 29] which is constrained to reproduce the electrode bulk density of states and to have the same Fermi energy as that of the system on which the DFT calculation was initially performed. The advantage of choosing a Bethe lattice resides in that the self-energies can be easily calculated through a well-known iteration procedure.[28, 29] For each atom in the outer planes of the cluster we choose to add a branch of the Bethe lattice in the direction

of any missing bulk atom. Once the Green's functions have been calculated we proceed to self-consistency by recalculating the elements of the density matrix P_{kl} according to:

$$P_{kl} = -\frac{1}{\pi} \int_{-\infty}^{\epsilon_F} \mathrm{Im} \left[\sum_{mn} S^{-1}_{km} G^r_{mn}(\epsilon) S^{-1}_{nl} \right] \mathrm{d}\epsilon \tag{5}$$

where ϵ_F is the Fermi level fixed by ensuring neutrality in the cluster, with S and G^r being the overlap and retarded Green's function matrices evaluated in a non-orthogonal atomic basis set. The new density matrix is used to recalculate the finite cluster Hamiltonian matrix, and the whole process is repeated until self-consistency is achieved.

A final remark regarding the comparison between the experimental conductance profile and the one calculated by us must be made. Strictly speaking only the conductance at the Fermi level should be comparable with the experimental one, but the weak tip-C_{60} interaction guarantees that the conductance profile will not vary strongly with the applied voltage within the bias range used in the STM experiments. This fact allows for a comparison between curves in the left panel of Figure 1 and those of Figure 2, although at contact tip-fullerene distances the applied bias may produce non-trivial voltage drops. Extension of our method to cope with generic non-equilibrium situations is currently being implemented.

References

[1] Rogero, C.; Pascual, J. I.; Gómez-Herrero, J.; Baró, A. M. *J. Chem. Phys.* **2002**, *116*, 832–836.

[2] Bardeen, J. *Phys. Rev. Lett.* **1961**, *6*, 2654.

[3] Tersoff, J.; Hamann, D. R. *Phys. Rev. B* **1985**, *31*, 805–813.

[4] Lang, N. D. *Phys. Rev. B* **1986**, *34*, 5947–5950.

[5] Meunier, V.; Lambin, P. *Phys. Rev. Lett.* **1998**, *81*, 5588–5591.

[6] Joachim, C.; Gimzevski, J. K.; Schlittler, R. R.; Chavy, C. *Phys. Rev. Lett.* **1995**, *74*, 2102–2105.

[7] Hanna, A. E.; Tinkham, M. *Phys. Rev. B* **1991**, *44*, 5919–5922.

[8] Bar-Sadeh, E.; Goldstein, Y.; Zhang, C.; Deng, H.; Abeles, B.; Millo, O. *Phys. Rev. B* **1994**, *50*, 8961–8964.

[9] Porath, D.; Levi, Y.; Tarabiah, M.; Millo, O. *Phys. Rev. B* **1997**, *56*, 9829–9833.

[10] Datta, S. *Electronic transport in mesoscopic systems*; Cambridge University Press: Cambridge, 1995.

[11] Palacios, J. J.; Pérez-Jiménez, A. J.; Louis, E.; Vergés, J. A. *Phys. Rev. B* **2001**, *64*, 115411.

[12] Palacios, J. J.; Pérez-Jiménez, A. J.; Louis, E.; SanFabián, E.; Vergés, J. A. *Phys. Rev. B* **2002**, *66*, 35322.

[13] Palacios, J. J.; Pérez-Jiménez, A. J.; Louis, E.; SanFabián, E.; Vergés, J. A. *Nanotechnology* **2002**, *13*, 378–381.

[14] Wilson, R. J.; Meijer, G.; Bethune, D. S.; Johnson, R. D.; Chambliss, D. D.; Vries, M. S.de ; Hunziker, H. E.; Wendt, H. R. *Nature* **1990**, *348*, 621–622.

[15] Altman, E. I.; Colton, R. J. *Surf. Sci.* **1992**, *279*, 49–67.

[16] Altman, E. I.; Colton, R. J. *Surf. Sci.* **1993**, *295*, 13–33.

[17] Altman, E. I.; Colton, R. J. *Phys. Rev. B* **1993**, *48*, 18244–18249.

[18] Fujita, D.; Yakabe, T.; Nejoh, H.; Sato, T.; Iwatsuki, M. *Surf. Sci.* **1996**, *366*, 93–98.

[19] Tzeng, C.-T.; Lo, W.-S.; Yuh, J.-Y.; Chu, R.-Y.; Tsuei, K.-D. *Phys. Rev. B* **2000**, *61*, 2263–2272.

[20] Hashizume, T.; Motai, K.; Wang, X. D.; Shinohara, H.; Saito, Y.; Maruyama, Y.; Ohno, K.; Kawazoe, Y.; Nishina, Y.; Pickering, H. W.; Kuk, Y.; Sakurai, T. *Phys. Rev. Lett.* **1993**, *71*, 2959–2962.

[21] Ohno, T. R.; Chen, Y.; Harvey, S. E.; Kroll, G. H.; Weaver, J. H.; Haufler, R. E.; Smalley, R. E. *Phys. Rev. B* **1991**, *44*, 13747–13755.

[22] Chase, S. J.; Bacsa, W. S.; Mitch, M. G.; Pilione, L. J.; Lannin, J. S. *Phys. Rev. B* **1992**, *46*, 7873–7877.

[23] Park, H.; Park, J.; Lim, A. K. L.; Anderson, E. H.; Alivisatos, A. P.; McEuen, P. L. *Nature* **2000**, *407*, 57–60.

[24] Frisch, M. J.; Trucks, G. W.; Schlegel, H. B.; G. E. Scuseria, M. A. R.; Cheeseman, J. R.; Zakrzewski, V. G.; Montgomery, J. A.; Jr., ; Stratmann, R. E.; Burant, J. C.; Dapprich, S.; Millam, J. M.; Daniels, A. D.; Kudin, K. N.; Strain, M. C.; Farkas, O.; Tomasi, J.; Barone, V.; Cossi, M.; Cammi, R.; Mennucci, B.; Pomelli, C.; Adamo, C.; Clifford, S.; Ochterski, J.; Petersson, G. A.; Ayala, P. Y.; Cui, Q.; Morokuma, K.; Malick, D. K.; Rabuck, A. D.; Raghavachari, K.; Foresman, J. B.; Cioslowski, J.; Ortiz, J. V.; Baboul, A. G.; Stefanov, B. B.; Liu, G.; Liashenko, A.; Piskorz, P.; Komaromi, I.; Gomperts, R.; Martin, R. L.; Fox, D. J.; Keith, T.; Al-Laham, M. A.; Peng, C. Y.; Nanayakkara, A.; Gonzalez, C.; Challacombe, M.; Gill, P. M. W.; Johnson, B.; Chen, W.; Wong, M. W.; Andres, J. L.; Gonzalez, C.; Head-Gordon, M.; Replogle, E. S.; Pople, J. A., GAUSSIAN98, Revision A.7, Gaussian, Inc., Pittsburgh PA, 1998.

[25] Becke, A. D. *J. Chem. Phys.* **1993**, *98*, 1372–1377.

[26] Palacios, L. F.; Christiansen, P. A. *J. Chem. Phys.* **1985**, *82*, 2664–.

[27] Roos, R. B.; Powers, J. M.; Atashroo, T.; Ermler, W. C.; LaJohn, L. A.; Christiansen, P. A. *J. Chem. Phys.* **1990**, *93*, 6654.

[28] Louis, E.; Yndurain, F. *Phys. Rev. B* **1977**, *16*, 1542.

[29] Martín-Moreno, L.; Vergés, J. A. *Phys. Rev. B* **1990**, *42*, 7193.

FIG. 1: Left panel: Normalized conductance derived from CITS measurements by Rogero *et al.*[1] for the two types of C_{60} adsorption sites on Au(111). Right panel: CITS image by Rogero *et al.*[1] at a bias of +0.6V, where the difference in brightness between on-top and bridge sites is clearly seen. The circle and triangle indicate the points where the curves shown in the left panel were obtained. The Fermi level is set to zero. The above pictures are reprints of Figs. 4d) and 4c) appearing in *The Journal of Chemical Physics*, Vol. 116, No. 2, pp. 832-836.

FIG. 2: Conductance spectra calculated with our method for the on-top and bridge adsorption sites in the region around the Fermi level (here set to zero). The inset shows the same data for the on-top geometry on a wider energy range, where the fullerene gap can be clearly appreciated.

FIG. 3: Cluster model used to represent the relevant part of the tip-C_{60}-surface system. The fullerene is oriented with an hexagon facing a bridge site of the Au(111) surface.

FIG. 4: Same as in Figure 3 for the on-top geometry.

FIG. 5: DFT Potential Energy Scan of a C_{60} molecule approaching the two types of Au(111) surface sites (On-top and Bridge). Results with an hexagon and a pentagon of the fullerene facing the surface are included for complete-

ness. The energy of the separated C_{60} + surface is set to zero.

FIG. 6: Top panel: Conductance profile from tunneling to contact regime of a C_{60} molecule adsorbed on top of a gold atom in a Au(111) surface. Bottom panel: Same as above for the C_{60} molecule adsorbed on a bridge site in a Au(111) surface. Distance (in Angstrom) between gold surface and tip displayed in the legend. The Fermi level has been set to zero in both sets of curves. The inset in both panels plots the same data on a wider energy range at tip-surface distances of 13.5 and 14.5 Å.

FIG 7: Maximum conductance from the second peak of Figure 6 for both geometries. The tunneling regime can be distinguished by the exponential decay in the conductance beyond 13Å. The inset shows the same data with a logarithmic scale for the conductance.

Figure 1:

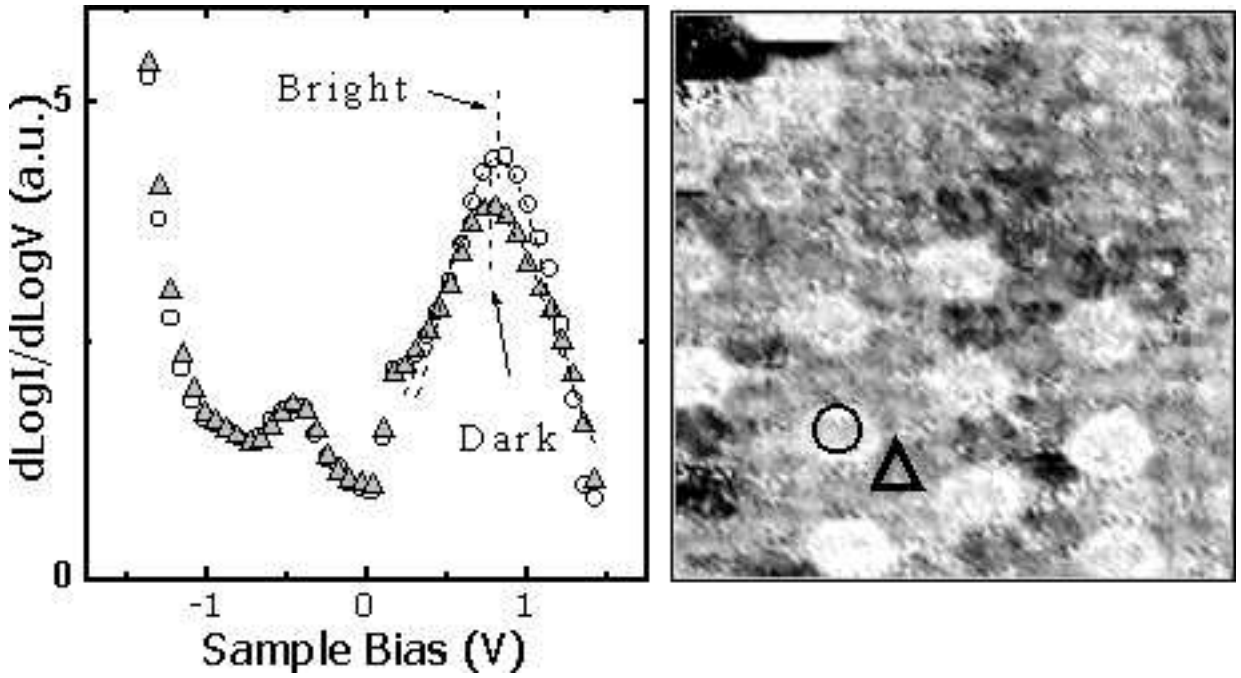

Figure 2:

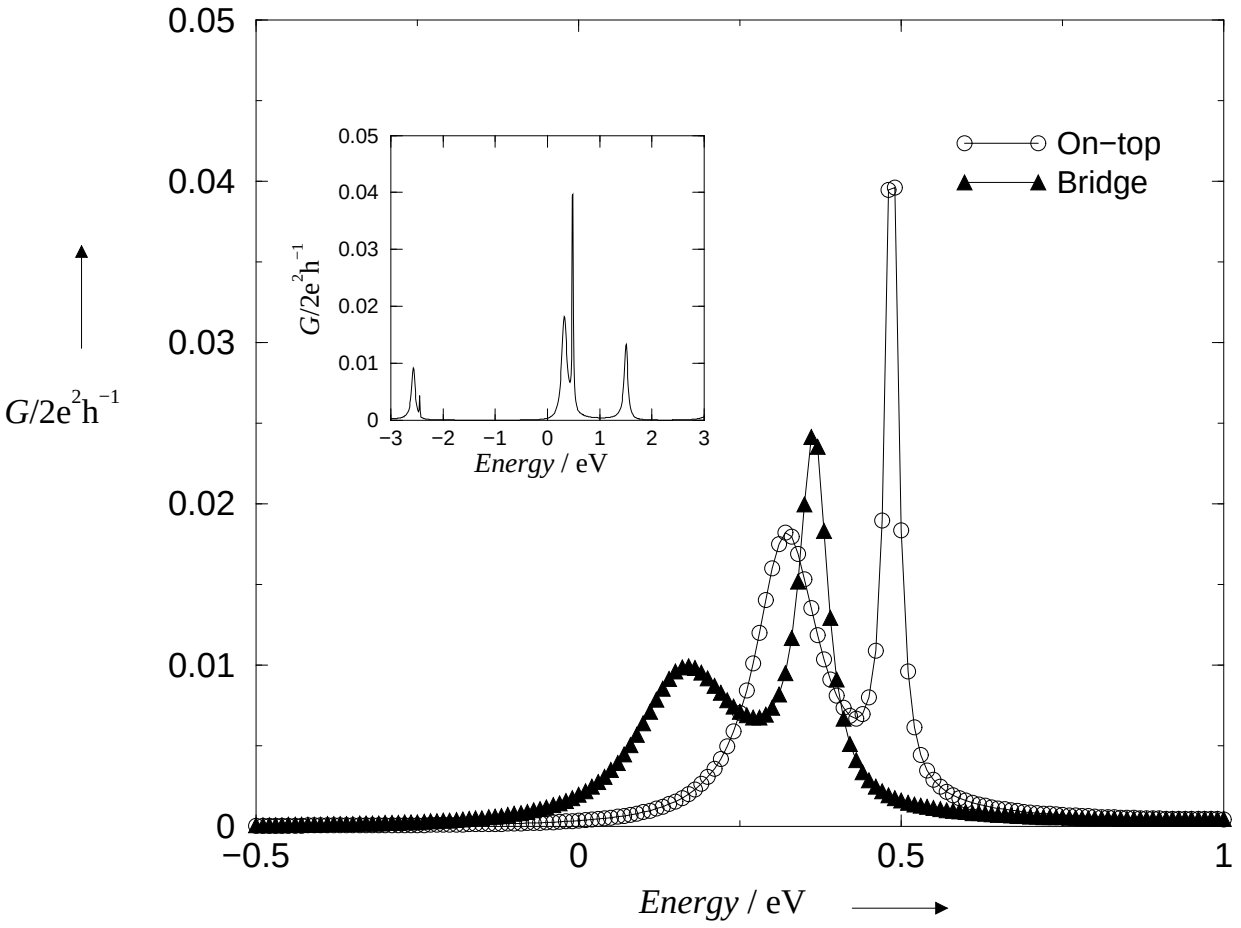
0.05
0.04
0.03
0.02
0.01
0
−0.5
0
0.5
1
$G/2e^2h^{-1}$
Energy / eV
On−top
Bridge
0.05
0.04
0.03
0.02
0.01
0
−3
−2
−1
0
1
2
3
$G/2e^2h^{-1}$
Energy / eV

Figure 3:

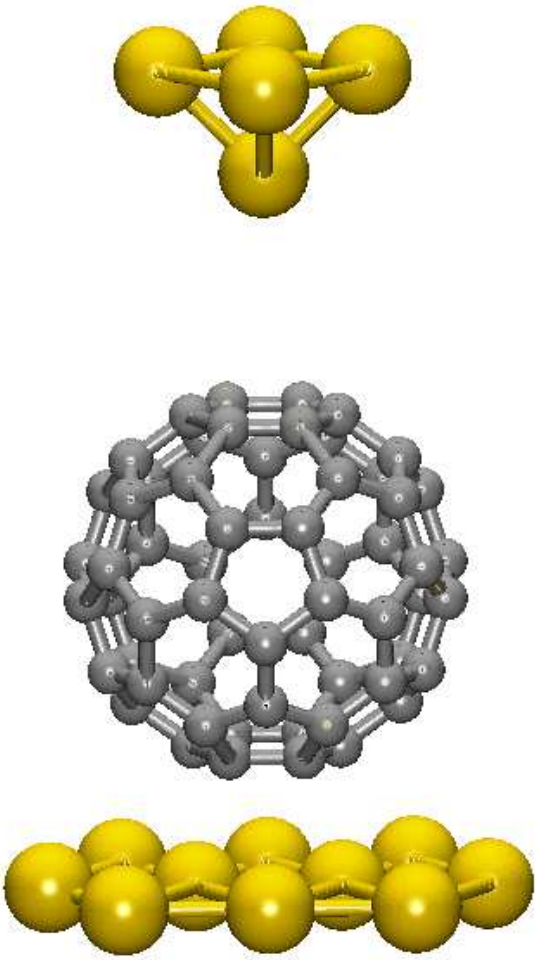

Figure 4:

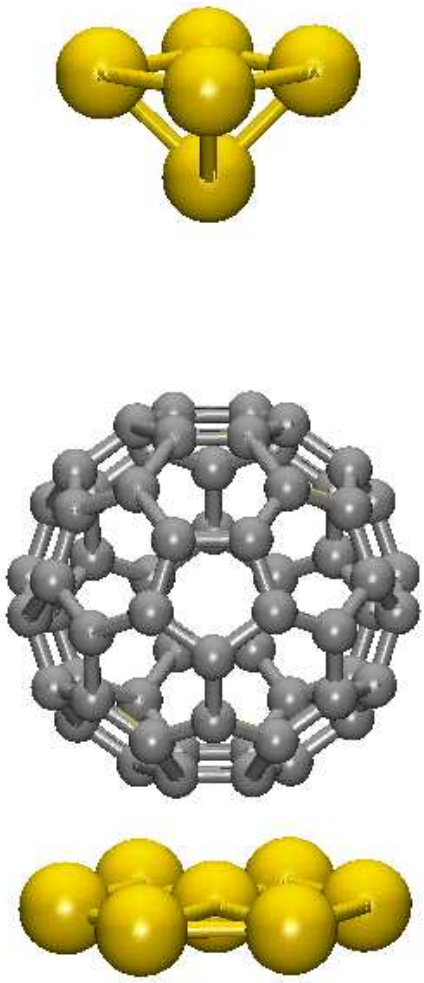

Figure 5:

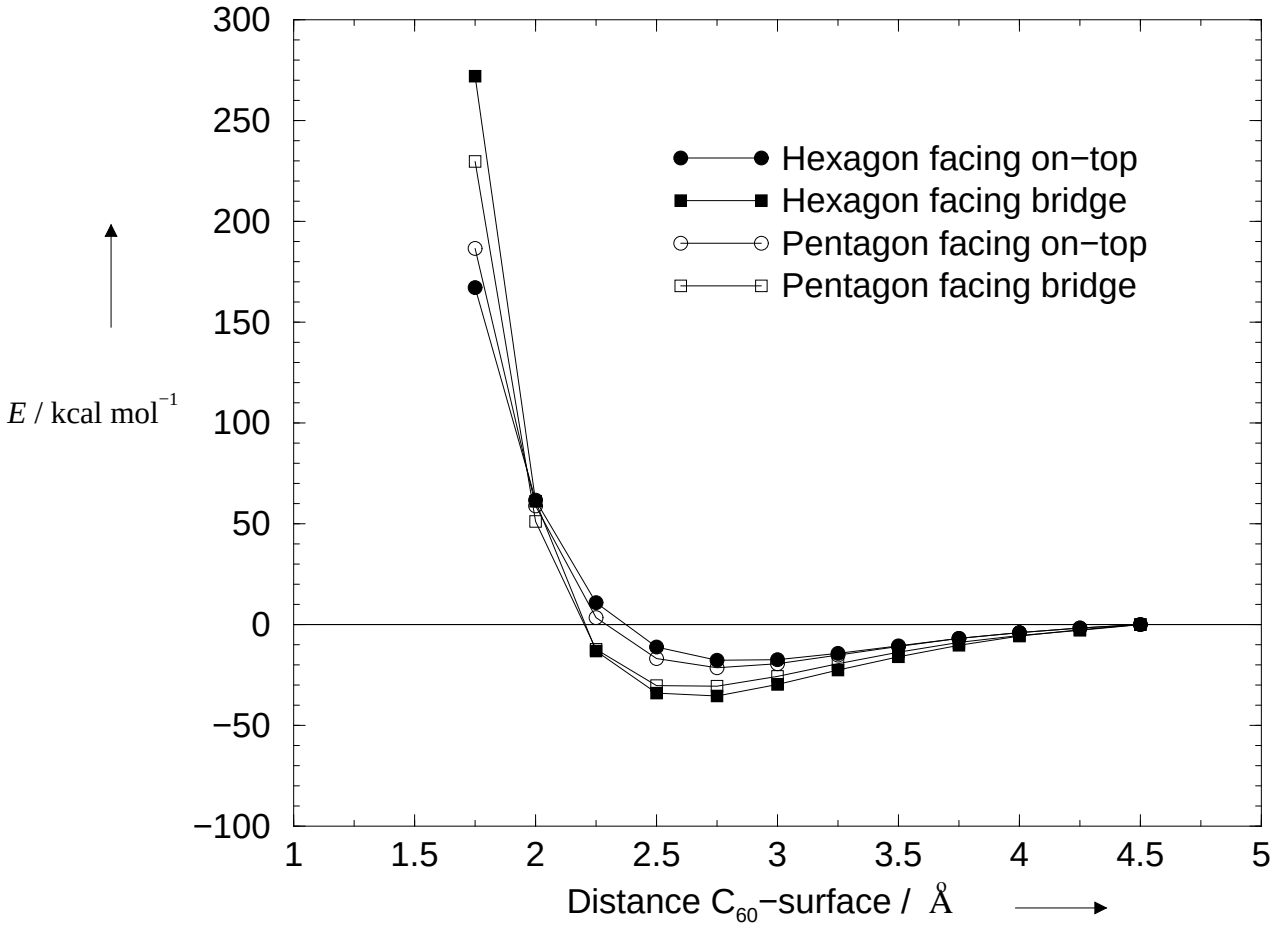
300
250
200
150
100
50
0
−50
−100
1
1.5
2
2.5
3
3.5
4
4.5
5
E / kcal mol−1
Distance C60−surface / Å
Hexagon facing on−top
Hexagon facing bridge
Pentagon facing on−top
Pentagon facing bridge

Figure 6:

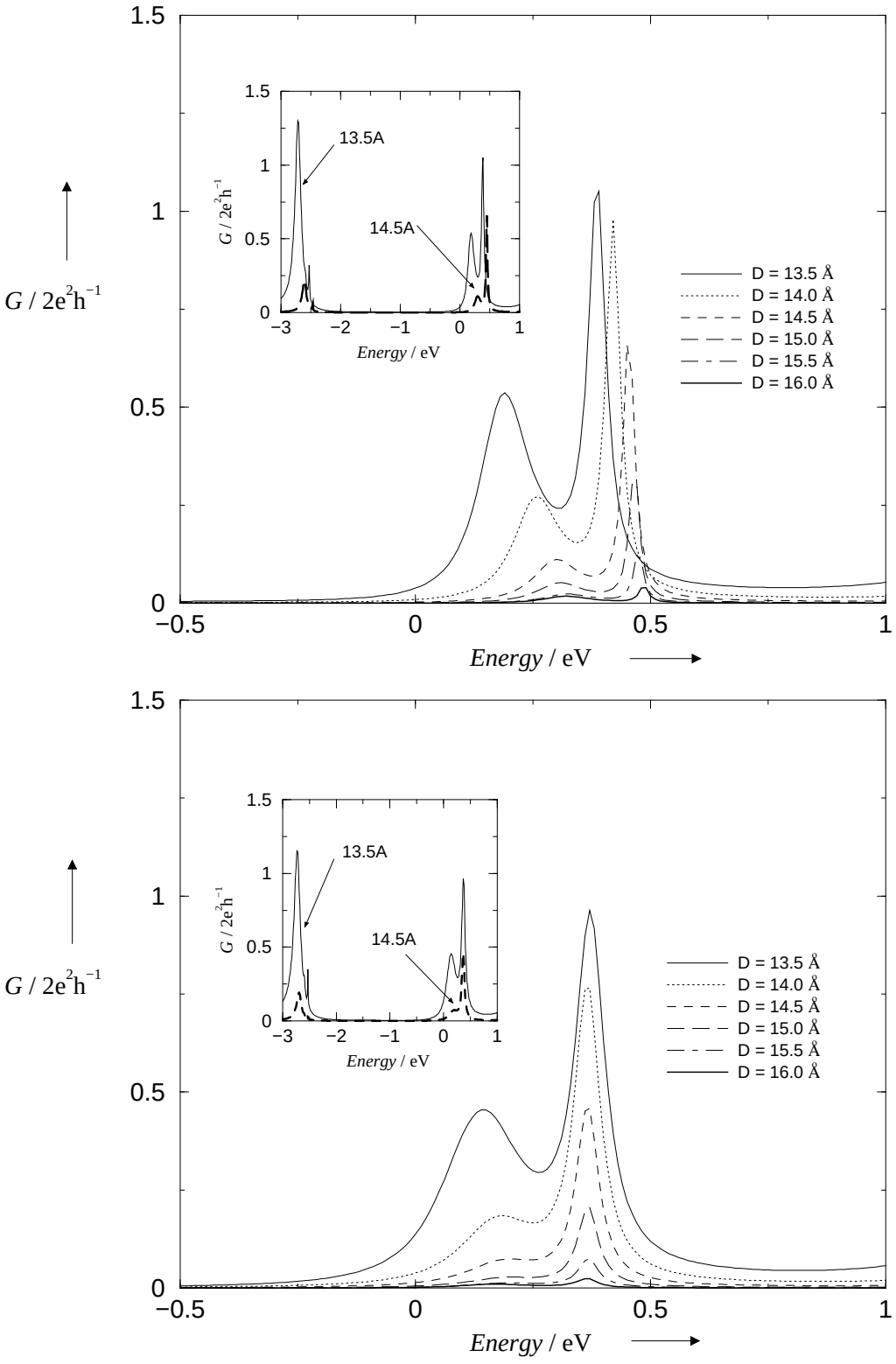
1.5
1
0.5
0
−0.5
0
0.5
1
G / 2e²h⁻¹
Energy / eV
13.5A
14.5A
D = 13.5 Å
D = 14.0 Å
D = 14.5 Å
D = 15.0 Å
D = 15.5 Å
D = 16.0 Å
−3
−2
−1

Figure 7:

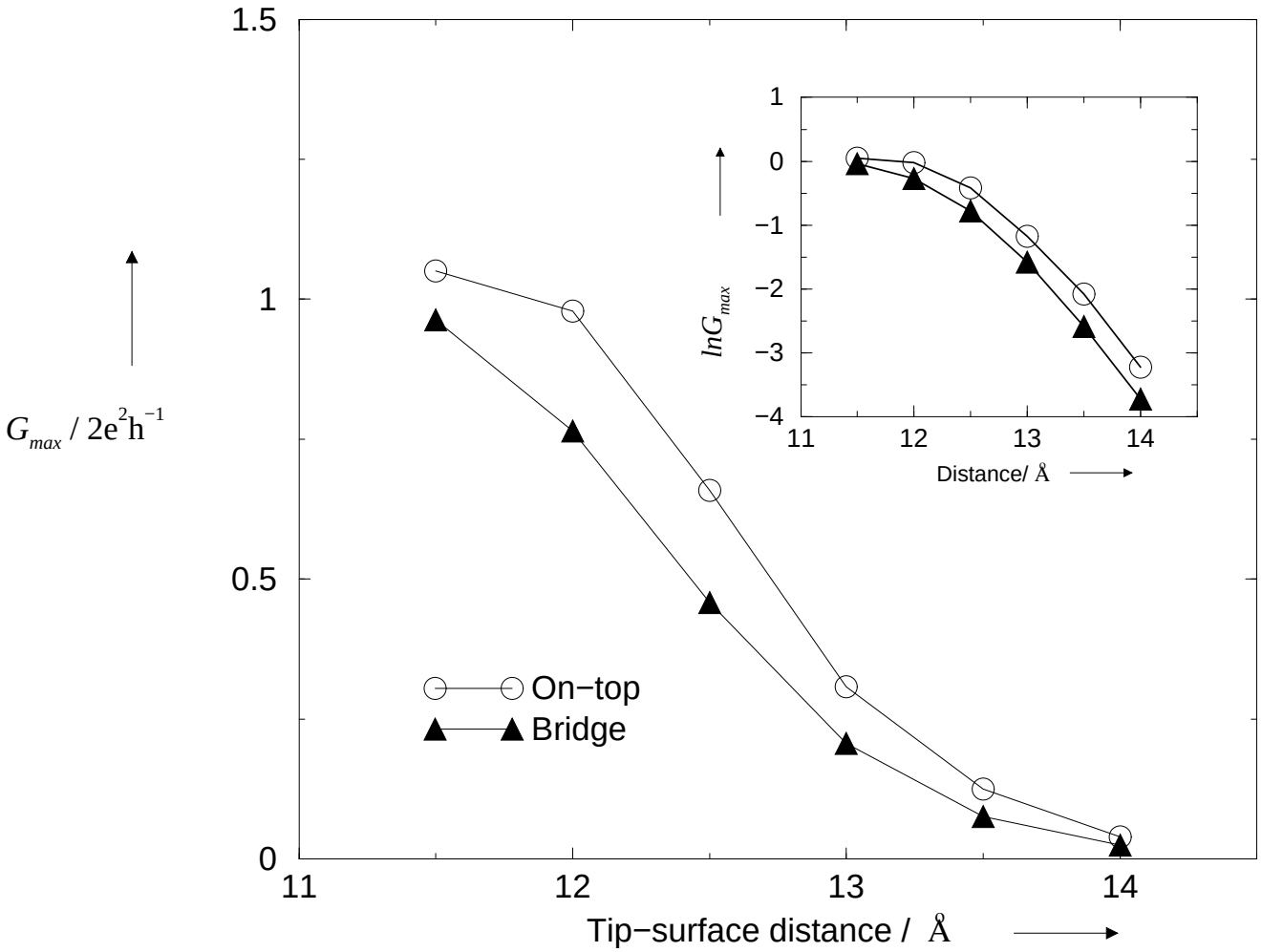
1.5
1
0.5
0
11
12
13
14
Tip−surface distance / Å
G_{max} / $2e^2h^{-1}$
On−top
Bridge
lnG_{max}
1
0
−1
−2
−3
−4
11
12
13
14
Distance/ Å